applied sciences

MDPI

Article

Evaluation of Antioxidant and Cytotoxicity Activities of Copper Ferrite ($CuFe_2O_4$) and Zinc Ferrite ($ZnFe_2O_4$) Nanoparticles Synthesized by Sol-Gel Self-Combustion Method

Samikannu Kanagesan [1,2,*], Mansor Hashim [1], Sidek AB Aziz [1,2], Ismayadi Ismail [1], Subramani Tamilselvan [3], Noorjahan Banu Alitheen [3], Mallappa Kumara Swamy [3,4] and Bandaru Purna Chandra Rao [5]

1 Materials Synthesis and Characterization Laboratory (MSCL), Institute of Advance Technology (ITMA), Universiti Putra Malaysia, 43400 UPM Serdang, Selangor, Malaysia; mansorhashim@gmail.com (M.H.); sidekaziz@gmail.com (S.A.A.); kayzen@gmail.com (I.I.)

2 Department of Physics, Faculty of Science, Universiti Putra Malaysia, 43400 UPM Serdang, Selangor, Malaysia

3 Department of Cell and Molecular Biology, Faculty of Biotechnology and Biomolecular Sciences, Universiti Putra Malaysia, 43400 Serdang, Selangor, Malaysia; drstamilselvan@gmail.com (S.T.); noorjahan@upm.edu.my (N.B.A.); swamy.bio@gmail.com (M.K.S.)

4 Department of Crop Science, Universiti Putra Malaysia (UPM), 43400 Serdang, Selangor, Malaysia

5 Department of Applied Science and Humanities, Sasi Intitute of Technology and Engineering, Tadepalligudem, West Godavari District-534101, Andhra Pradesh, India; nanopurna@gmail.com

* Correspondence: kanagu1980@gmail.com; Tel.: +6010-4374-970

Academic Editor: Philippe Lambin

Received: 28 December 2015; Accepted: 2 March 2016; Published: 30 August 2016

Abstract: Spinel copper ferrite ($CuFe_2O_4$) and zinc ferrite ($ZnFe_2O_4$) nanoparticles were synthesized using a sol-gel self-combustion technique. The structural, functional, morphological and magnetic properties of the samples were investigated by Fourier transform infrared spectroscopy (FTIR), X-ray diffraction (XRD), Transmission electron microscopy (TEM) and vibrating sample magnetometry (VSM). XRD patterns conform to the copper ferrite and zinc ferrite formation, and the average particle sizes were calculated by using a transmission electron microscope, the measured particle sizes being 56 nm for $CuFe_2O_4$ and 68 nm for $ZnFe_2O_4$. Both spinel ferrite nanoparticles exhibit ferromagnetic behavior with saturation magnetization of 31 $emug^{-1}$ for copper ferrite (50.63 Am^2/Kg) and 28.8 Am^2/Kg for zinc ferrite. Both synthesized ferrite nanoparticles were equally effective in scavenging 2,2-diphenyl-1-picrylhydrazyl hydrate (DPPH) free radicals. $ZnFe_2O_4$ and $CuFe_2O_4$ nanoparticles showed 30.57% ± 1.0% and 28.69% ± 1.14% scavenging activity at 125 μg/mL concentrations. In vitro cytotoxicity study revealed higher concentrations (>125 μg/mL) of $ZnFe_2O_4$ and $CuFe_2O_4$ with increased toxicity against MCF-7 cells, but were found to be non-toxic at lower concentrations suggesting their biocompatibility.

Keywords: copper ferrite; zinc ferrite; nanoparticles; cytotoxic

1. Introduction

For some time, magnetic fine nanoparticles have been of major research interest because of their technological importance. Among the whole magnetic family, spinel type magnetic ferrites, MFe_2O_4 (M = Mn, Ca, Mg, Zn, Ni, Co, Cd. etc.) [1–6], have great importance in electronic, magnetic and especially biomedical applications as well as in modern technologies. Spinel ferrites are used in a broad range of applications; magnetic refrigeration, Ferro fluids, high density recording, spintronics,

drug delivery, bio sensors, magnetic resonance imaging and magnetic hydrothermia [7–16]. Copper ferrite is a ferromagnetic material that crystallizes in tetragonal spinel with space group I41/amd, and forms a crystal system based on the anti-parallel alignment of the magnetic moments of A and B sub lattices. $ZnFe_2O_4$ is one of the most commonly studied materials. It crystallizes in the spinel structure with octahedral B sites occupied by Fe^{3+} and the tetrahedral A sites preferentially occupied by Zn^{2+}. Nowadays, nanoparticles have gained more attention because of their extraordinary properties, differing from bulk materials [17–20]. It is well known fact that material properties majorly depend on the different method of synthesis. For spinel ferrite synthesis, physical and chemical approaches are reported such as sol-gel, flash combustion, citrate gel, co-precipitation, hydrothermal synthesis, sol-gel auto combustion method, and micro-emulsion [17–19,21–27]. Among all the different synthesis roots, co-precipitation [28] and sol-gel combustion [29] allow good control over particle size and uniform distribution, enhancing the extraordinary properties of ferrites. The sol-gel self-combustion technique is an effective method to produce small and uniform particles at low temperatures [30].

More recently, considerable attention has been paid to magnetic nanoparticles due to their prospective applications in the field of biomedicine, biotechnology, material science and engineering. These nanoparticles exhibit good magnetic properties as well as various molecular and cellular level interactions in several biological processes [31]. Magnetic nanoparticles are highly preferable; being biocompatible, they are relatively less toxic and possess magnetic properties [32,33]. Free radicals are molecules or atoms with an unpaired electron. These are highly reactive species that destabilize other molecules and produce many more free radicals. In biological systems, free radicals are formed as a part of the body's normal metabolic processes when biomolecules interact with oxygen. However, increased levels of free radicals are detrimental to human health as they cause several disorders, including cancer, myocardial infarction, atherosclerosis, and neurodegenerative disorders [34]. Chemical substances, known as antioxidants, can scavenge these free radicals and, thus, decrease the occurrence of oxidative stress induced cell death or damage. Researchers have proved that nanoparticles can act as synthetic antioxidants in the body and possess good antioxidant properties compared to their bulk material counterparts, which is attributed to the increased surface to volume ratio of the nanostructures [35–37]. Similarly, the increased surface area of nanoparticles can be properly functionalized to bind specifically to cancerous cells and, thus, offer an approach for cancer therapy. Moreover, it has been stated that drug delivery systems using nanoparticles are very efficient in the treatment of cancer because of their superior bio-distribution profile and pharmacokinetics [38]. However, potential applications of nanoparticles can be considered practically only when their toxic effect is understood. Though various ferrite nanoparticles are synthesized and characterized, their biological activities including cytotoxicity are not well explored yet. To date, very little information is available on the toxicity of magnetic nanoparticles [30,39–41]. In recent times, research has been focused on the improvement of the magnetic properties of nanomaterials by modifying their chemical structure, size and shape. In this regard, we have successfully synthesized novel $CuFe_2O_4$ and $ZnFe_2O_4$ nanoparticles and evaluated their structural, magnetic, antioxidant and cytotoxicity properties.

2. Experimental Section

2.1. Preparation of $CuFe_2O_4$ and $ZnFe_2O_4$ Nanoparticles

Analytical grade copper nitrate (Sigma-Aldrich Corporation, St. Louis, MO, USA), ferric nitrate (Sigma-Aldrich Corporation, St. Louis, MO, USA) and citric acid (Sigma-Aldrich Corporation, St. Louis, MO, USA) were purchased from Aldrich chemicals. Copper nitrate and ferric nitrate in the molar ratio of 1:2, and citric acid in the ratio of 1:1 with nitrates were dissolved in a minimum amount of ethanol (Systerm, Shah Alam-40150, Selangor Darul Ehsan, Malaysia). A suitable amount of oleic acid (Sigma-Aldrich Corporation, St. Louis, MO, USA) was added to the solution. The solution was stirred for 4 h at room temperature and kept in a vacuum rotary evaporator (Renetech, Semenyih, Selangor Darul Ehsan, Malaysia) at 60–80 °C to remove surplus water. The gel was heated at 150 °C in a hot air

oven for 24 h. A brown color ($CuFe_2O_4$) powder was obtained. The same procedure was followed for $ZnFe_2O_4$ nanoparticle preparation, but we used zinc nitrate instead of copper nitrate.

2.2. Characterization

X-ray diffraction pattern of the calcined powder sample was carried out by X-ray diffractometer (PANalyticalX'pert pro, Department of Marketing and Communications, Almelo, The Netherlands) with CuKα radiation at 45 kV and 40 mA (k = 0.15406 nm) in a wide range of 2θ ($20^\circ \leqslant 2\theta \leqslant 70^\circ$). The functional groups of copper ferrite and zinc ferrite powders were investigated in the 400–4000 /cm range with a Thermo Nicolet 6700 Fourier transform infrared spectrometer (FTIR, Thermo scientific, Waltham, MA, USA). The particle morphology observation of the specimen was performed using a Transmission electron microscope (TEM, JEM 3010-JEOL, Sollentuna, Sweden) with an accelerating voltage of 200 kV. The magnetic characteristics of the specimen were measured at room temperature, with a maximum field of 20,000 Gauss using a Lakeshore vibrating sample magnetometer (VSM) (LakeShore 7407, Lake Shore Cryotronics, Inc, Westerville, OH, USA).

2.3. Antioxidant Activity (Evaluation of DPPH Free Radical Scavenging Activity)

The antioxidant activity of $CuFe_2O_4$ and $ZnFe_2O_4$ nanoparticles was evaluated by means of 2,2-diphenyl-1-picrylhydrazyl hydrate (DPPH) free radical scavenging assay [34]. In brief, varied concentrations of $CuFe_2O_4$ or $ZnFe_2O_4$ nanoparticles (25, 50, 75, 100 and 125 µg/mL) were added to 10 mL of 0.1 mM DPPH (Sigma-Aldrich, St. Louis, MO, USA) solution and placed under dark at room temperature for 30 min to facilitate the reaction. Thereafter, using ethanol as blank, the absorbance was recorded at 517 nm wavelengths. The experiment was conducted in a similar manner using ascorbic acid (Sigma-Aldrich, St. Louis, MO, USA) as standard. Scavenging activity was determined based on the absorbance i.e., the lower the absorbance, the higher is the scavenging activity. The percentage inhibition of free radicals was calculated based on the formula given below:

$$\%\,\text{inhibition}\,\frac{Control\ OD - Sample\ OD}{Control\ OD} \times 100 \quad (1)$$

2.4. Evaluation of Cytotoxicity Activity

We evaluated the cytotoxic effect of $CuFe_2O_4$ and $ZnFe_2O_4$ nanoparticles on the human breast cancer cell line (MCF-7) as described previously by Swamy et al. [35]. Briefly, the cells were cultured on DMEM (Dulbecco's Modified Eagles Medium) (Sigma-Aldrich, St. Louis, MO, USA) added with L-glutamine (2 mM) (PAA Laboratories GmbH, Pasching, Austria), penicillin (100 U/mL) (Sigma-Aldrich, St. Louis, MO, USA), streptomycin (100 µg/mL) (Sigma-Aldrich, St. Louis, MO, USA) and fetal bovine serum (10%) (PAA Laboratories GmbH, Pasching, Austria). Approximately 5×10^4 cells were inoculated in each well of 96-well plates (Nunc A/S, Roskilde, Denmark, Denmark) and incubated in a carbon dioxide incubator (Contherm Scientific Ltd, Lower Hutt, New Zealand) maintained at 37 °C for 48 h. For the cytotoxicity test, the cells were challenged with $CuFe_2O_4$ or $ZnFe_2O_4$ nanoparticles (0, 15.625, 31.25, 62.5, 125, 250 and 500 µg/mL) and incubated for 24 h, 48 h and 72 h separately to study cell viability using 3-(4,5-dimethylthiazol-2-yl)-2,5-diphenyltetrazolium bromide (MTT) assay (Sigma-Aldrich, St. Louis, MO, USA). About 20 µL of MTT solution (5 mg/mL) was added to each well and further kept for 4 h of incubation under the same conditions and, using a multi-well ELISA plate reader (Bio-tech Instruments, Winooski, VT, USA), absorbance was recorded at 570 nm. The absorbance was converted to percentage of cell viability by using the following formula:

$$\%\,\text{of cell viability} = \frac{Values\ in\ the\ experimental\ samples}{Values\ of\ optical\ density\ in\ control\ sample} \times 100 \quad (2)$$

3. Results and Discussion

3.1. X-ray Diffraction (XRD) Analysis

Figure 1a,b represents the XRD pattern of the as synthesized $CuFe_2O_4$ and $ZnFe_2O_4$ nanoparticles. Respective diffraction peaks of hydrothermally synthesized $CuFe_2O_4$ sample peaks were observed and exactly coincide with the reported values (JCPDS file No.: 34-0425). The exhibited reflection peaks of diffraction planes were indexed from $ZnFe_2O_4$ (JCPDS 82-1042). The crystal size of the as synthesized powder samples was measured by using De-Bye Scherer's formula:

$$(D = (\frac{(0.9\lambda)}{\beta\cos(\theta)}) \quad (3)$$

where D is the average crystalline size of the particle, λ is the incident wavelength, θ is the Brags angle and β is the diffracted full width at half maxima. The $CuFe_2O_4$ sample (Figure 1a) crystal-line size was calculated for the seven most intensely marked diffraction peaks (θ = 15.216, 16.602, 17.916, 21.790, 27.045, 28.802, 31.654), and the corresponding calculated values are 16.20, 35.55, 42.66, 35.82, 36.18, 31.25, and 22.47 nm, respectively. The $ZnFe_2O_4$ samples (Figure 1b) crystal-line size was calculated for the six most intensely marked diffraction peaks (θ = 15.153, 17.824, 21.651, 26.879, 28.601, 31.402), and the corresponding calculated values are 42.95, 32.32, 32.51, 10.96, 43.93, and 21.77 nm, respectively. The average crystalline size of $CuFe_2O_4$ and $ZnFe_2O_4$ was found to be about 31.42 nm and 30.74 nm, respectively. Clearly broadened X-ray diffraction peaks indicate that the prepared particles are small in size.

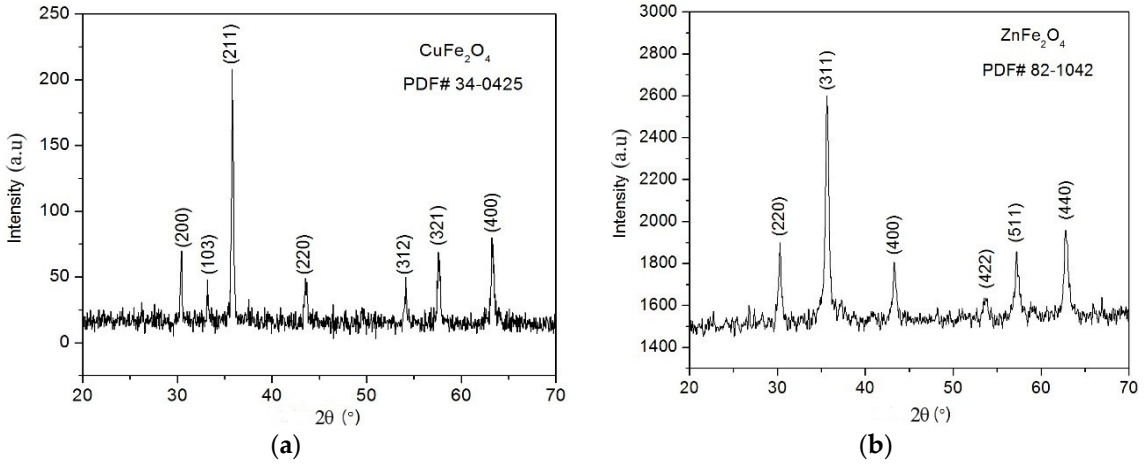

Figure 1. (**a**) X-ray Diffraction (XRD) pattern of the $CuFe_2O_4$ nanopowder; (**b**) XRD pattern of the $ZnFe_2O_4$ nanopowder.

3.2. FTIR Spectra Analysis

The FTIR spectra of the calcined copper ferrite and zinc ferrite samples are shown in Figure 2a,b. The wide band around 3425 in Figure 2a and 3447 in Figure 2b and absorption peaks at 1652 in Figure 2a and 1633 in Figure 2b correspond to the respective hydroxyl group [41,42]. A sharp peak around 1388 cm^{-1} in both the spinel ferrites is attributed to the symmetric vibration of the NO_3^- group [41]. The small absorption peaks around 2927 and 2855 cm^{-1} in zinc ferrite are ascribed to the anti-symmetric and symmetric-CH_2-vibrations of the carbon chains [43]. Generally, the metal oxide vibrations occur below 1000 cm^{-1} [41]. Fe–O–H bending vibrations were observed at 797 cm^{-1} [44]. The little broad band that presents at 552 cm^{-1} is marked as Fe–O vibration [45].

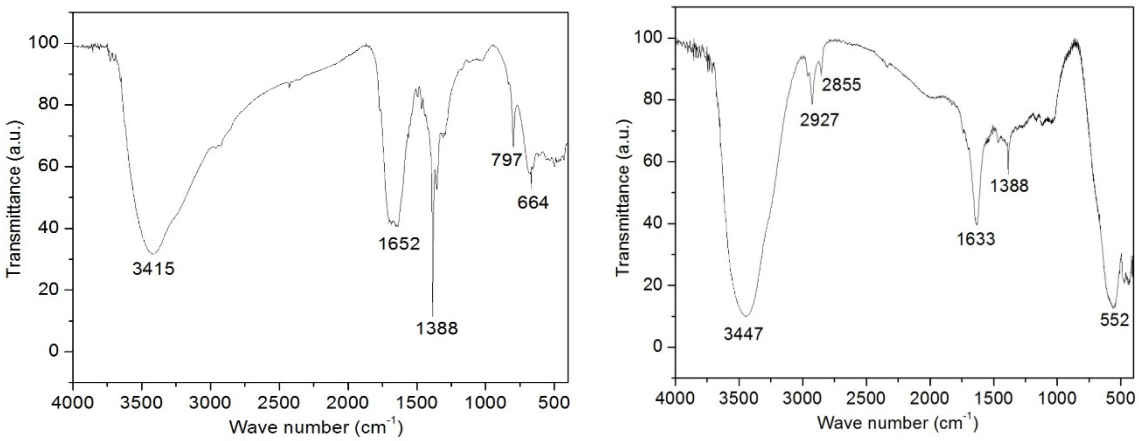

Figure 2. (**a**) Fourier transform infrared spectroscopy (FTIR) spectra of copper ferrite powder calcined at 150 °C for 24 h; (**b**) FTIR spectra of zinc ferrite powder calcined at 150 °C for 24 h.

3.3. Morphological Analysis

The particle size, shape and morphology of the as-prepared nickel ferrite nanoparticles were investigated through Transmission electron microscope (TEM). Figure 3a,b shows a typical TEM images of as synthesized $CuFe_2O_4$ and $ZnFe_2O_4$ nanoparticles. TEM images show that the $CuFe_2O_4$ and $ZnFe_2O_4$ nanoparticles have nearly spherical morphology, almost uniform size and distribution. The average particle size is found to be 56 nm for $CuFe_2O_4$ and 68 nm $ZnFe_2O_4$, respectively. Spinel ferrite particles generally have a spherical shape with smooth surfaces and a narrow size distribution [41,46].

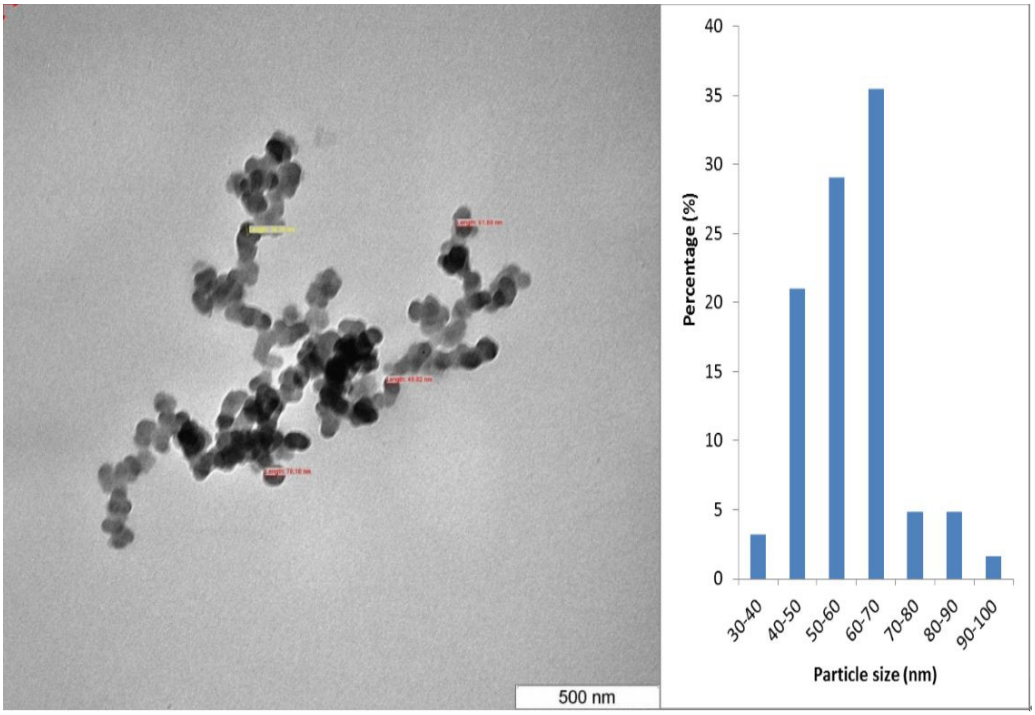

(**a**)

Figure 3. *Cont.*

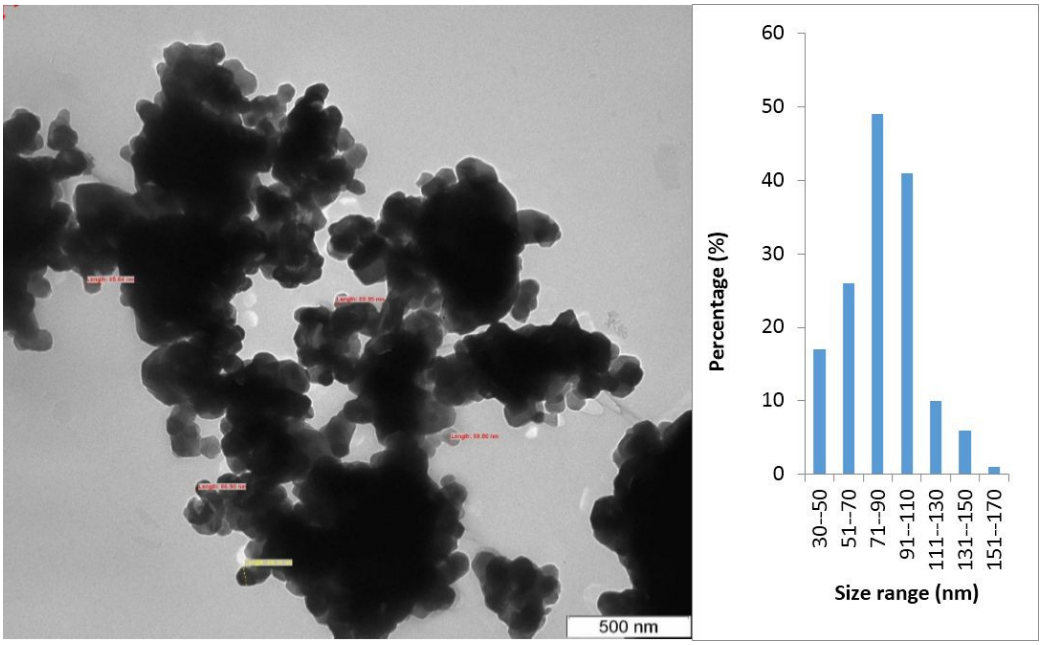

(**b**)

Figure 3. (**a**) Transmission electron microscope (TEM) image of calcined copper ferrite powder and the corresponding particle size histogram; (**b**) TEM image of calcined zinc ferrite powder and the corresponding particle size histogram.

3.4. Magnetic Analysis

Figure 4a,b shows the room-temperature magnetic hysteresis loops of the $CuFe_2O_4$ and $ZnFe_2O_4$ nanoparticles prepared by the sol-gel self-combustion technique. The Magnetic hysteresis (M–H) curve gives the information about the magnetic parameters such as saturation magnetization (Ms) and coercivity (Hc). Normally, the magnetization in spinel ferrites arises due to the difference in the magnetic moments of cations which are distributed in the octahedral and tetrahedral sites. From the literature review data, when the particle diameter is 50 nm or less, the particles appear to have superparamagnetic character. However, in our case, particle size is found to be 56 nm for $CuFe_2O_4$ and 68 nm $ZnFe_2O_4$, respectively. Both copper ferrite and zinc ferrite samples exhibit ferromagnetic behavior (see inset Figure 1a,b) at room temperature with saturation magnetization for $ZnFe_2O_4$ (28.8 Am^2/Kg) and $CuFe_2O_4$ (50.63 Am^2/Kg), respectively. The low value of Ms in both samples is due to the presence of very small sized particles. Generally, magnetic properties varied by varying the particle size, shape and crystallinity, etc. The observed value of saturation magnetization for $ZnFe_2O_4$ (28.8 Am^2/Kg) was significantly lower than the reported bulk $MgFe_2O_4$, $CuFe_2O_4$ and $NiFe_2O_4$ spinel ferrites (41.7, 45.7 and 49.1 emu/g, respectively) [47,48] but higher than $CuFe_2O_4$ (50.63 Am^2/Kg). These values are generally expected for nanosized materials. From the hysteresis, small size zinc ferrite nanoparticles exhibited low saturation magnetization compares to copper ferrite nanoparticles. Saturation magnetization (Ms) is an intrinsic factor of magnetic nanoparticles; it is influenced by the crystalline structure, chemical composition and method of preparation. The difference in saturation magnetization between $CuFe_2O_4$ and $ZnFe_2O_4$ may be due to the structural morphology, particle size and crystallinity of the corresponding nanoparticles. It has been reported that the magnetic properties are dependent on the method of synthesis and heating treatment. The exhibited coercivity of $CuFe_2O_4$ and $ZnFe_2O_4$ nanoparticles is 215.11 Gauss and 58.97 Gauss, respectively, and the values are strongly dependent on size.

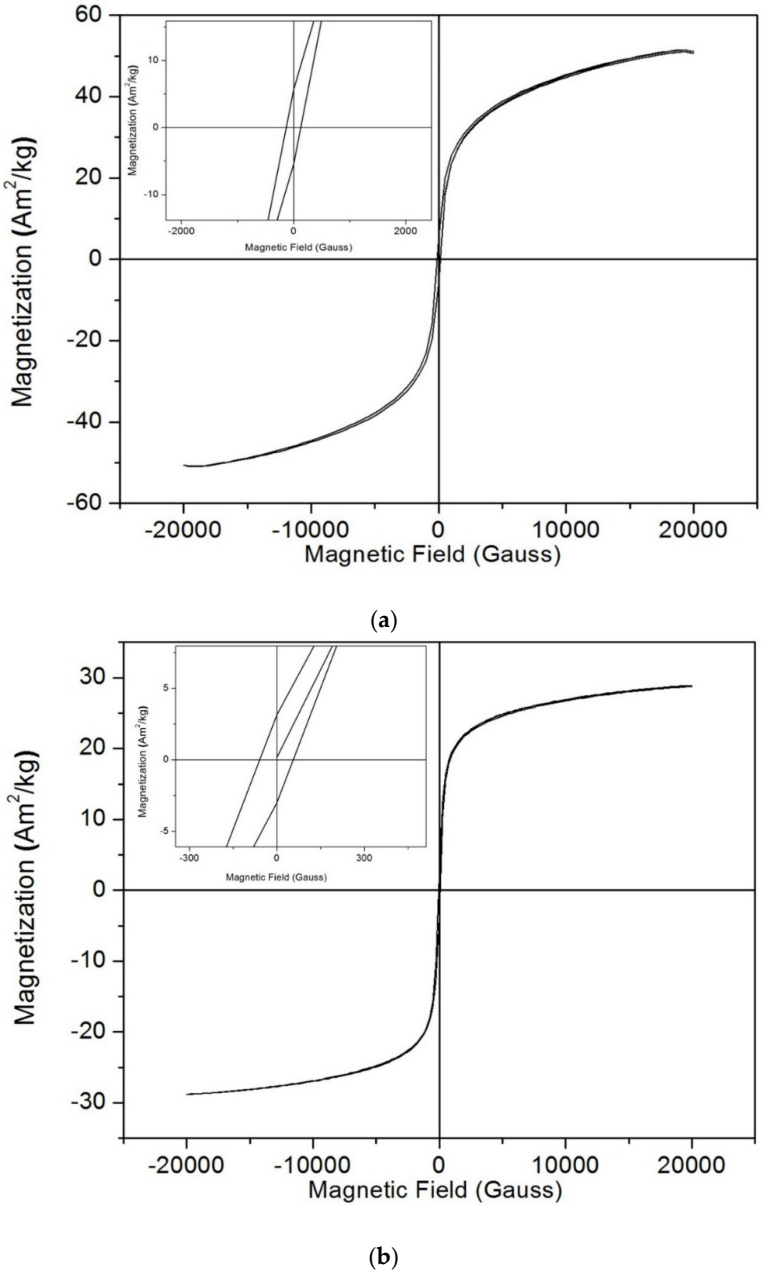

Figure 4. (**a**) Hysteresis loop of $CuFe_2O_4$ nanopowder at room temperature; (**b**) Hysteresis loop of $ZnFe_2O_4$ nanopowder at room temperature.

3.5. Antioxidant Activity

The biocompatibility of biomaterials is limited by oxidative stress that results in inflammation, chronic diseases and other problems. Hence, there is a need to design a material which possesses antioxidant properties in order to increase biocompatibility. DPPH free radical scavenging assay method was used to determine the antioxidant activity of $CuFe_2O_4$ and $ZnFe_2O_4$ nanoparticles. It is evident from the results that both $CuFe_2O_4$ and $ZnFe_2O_4$ nanoparticles exhibited potent antioxidant activity at different concentrations (Figure 5). However, between $CuFe_2O_4$ and $ZnFe_2O_4$, no significant difference was observed for antioxidant properties tested at all concentrations. However, free radical scavenging activities of both nanoparticles were inferior to the standard (ascorbic acid). The highest scavenging activity was observed in ascorbic acid (58.11% $\pm$ 1.52%) followed by $ZnFe_2O_4$ nanoparticles (30.57%) and $CuFe_2O_4$ nanoparticles (28.69% $\pm$ 1.14%) at 125 µg/mL concentration. With increased

doses of nanoparticles, the antioxidant activity was also increased correspondingly. This antioxidant activity could be linked to the transfer of free electrons from the oxygen atom of nanoparticles to free radicals present at the nitrogen atom of DPPH molecules. It has been reported that many of the metal nanoparticles can scavenge free radicals and act as antioxidants [49]. Moreover, a study by Das et al. (2013) [36] reported that the antioxidant activity is mainly due to high surface to volume ratio of the nanostructures. Similarly, ZnO nanoparticles have shown to possess 91% scavenging activity at 250 mg/mL concentration [50]. In another study, CuO nanoparticles at 120 mg/mL concentration showed 85% DPPH quenching activity [36]. Also, $CoFe_2O_4$, Fe_2O_4 and NiO nanoparticles were shown to exhibit relatively good antioxidant characteristics compared to their bulk materials [51–53]. However, systematic studies on the antioxidant properties of ferrite nanoparticles are not well documented. The result of our study is promising and provides a lead in the exploration of $CuFe_2O_4$ and $ZnFe_2O_4$ nanoparticles as a new source of antioxidants.

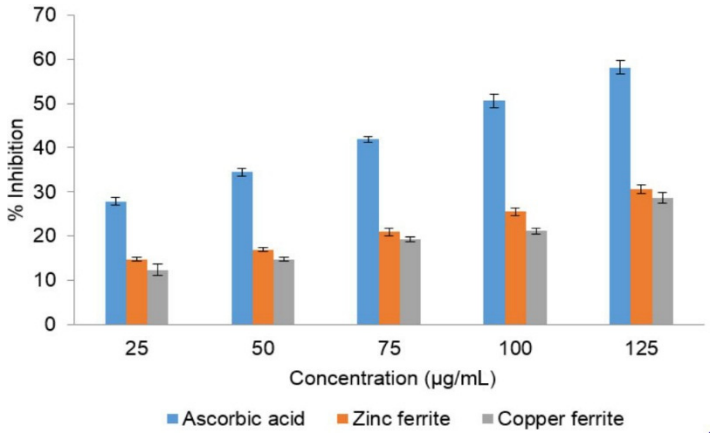

Figure 5. 2,2-diphenyl-1-picrylhydrazyl hydrate (DPPH) free radical scavenging activities of ascorbic acid, $CuFe_2O_4$ and $ZnFe_2O_4$ nanoparticles. Each value is expressed as a mean of ± Standard Deviation (S.D, $n = 3$).

3.6. Cytotoxicity Analysis

The cytotoxicity activity of $CuFe_2O_4$ and $ZnFe_2O_4$ nanoparticles at various concentrations against the MCF-7 cells (human breast adenocarcinoma cell line) using MTT assay is shown in Figure 6a,b. The results revealed the dose dependent cytotoxicity effect of both ferrite nanoparticles. The highest cell viability (100%) observed at 0 µg/mL began to decrease gradually with the increased concentrations and exposure time from 24 h to 72 h. The highest toxicity effect was observed at 500 µg/mL where 17% and 20% cell viability was observed after 72 h in $CuFe_2O_4$ and $ZnFe_2O_4$ nanoparticles, respectively, suggesting high toxicity at higher concentrations. Similarly, previous studies also have shown the dose dependent cytotoxicity of several types of nanoparticles [20,35,37,54,55]. Interestingly, both nanoparticles were observed to be less toxic at lower concentrations up to 100 µg/mL where about 80% of the cells were viable. However, both nanoparticles' concentrations above 125 µg/mL exhibited higher toxicity towards MCF-7 cells. For $CuFe_2O_4$ nanoparticles, the concentration which inhibits 50% of the cellular growth (IC_{50}) value was observed to be 415, 320 and 260 µg/mL after 24 h, 48 h and 72 h of incubation, respectively. While, $ZnFe_2O_4$ nanoparticles exhibited IC_{50} value of 310, 285 and 221 µg/mL after 24 h, 48 h and 72 h of incubation, respectively. This clearly suggests that $ZnFe_2O_4$ nanoparticles possess more toxicity compared to $CuFe_2O_4$ nanoparticles. This differential activity could be because of differences in their size, surface to volume ratio, shape as well as the magnetic properties as discussed in the earlier sections. Similarly, it has been reported that nanoparticles prepared from different bulk materials explicate their actions which mainly depends on the chemical composition as well as their sizes and shapes [56]. Our study is in agreement with the earlier reports where $CaFe_2O_4$ nanoparticles were shown to exhibit high toxicity when used above 250 µg/mL

concentration [40], while $MnFe_2O_4$, $ZnFe_2O_4$, $NiFe_2O_4$ nanoparticles at 100 µg/mL concentration have shown less cell viability [57,58]. Gupta et al. (2005) [59] stated that the magnetic nanoparticles size ranging from 10 to 100 nm is considered to be ideal for their application in the biomedical field. This is due to easy infiltration into cells, increased surface area for attachment and high permeability in solution [31]. The high surface area of the nanoparticles means superior physico-chemical and mechanical characteristics compared to their bulk materials. In this study, we obtained $ZnFe_2O_4$ and $CuFe_2O_4$ nanoparticles with sizes of 56 and 68 nm, respectively, which is well within their capacity. The mechanism of these nanoparticles may be attributed to the generation of reactive oxygen species (ROS) due to increased intracellular Cu^{2+} and Zn^{2+} resulting in the subsequent failure of cellular redox machinery [60]. Recently, protein corona-$ZnFe_2O_4$ nanoparticles were reported to show lower cytotoxic effects with improved therapeutic effects [61]. Also, superparamagnetic $ZnFe_2O_4$ based nanostructures were used in magneto-photothermal therapy of prostate cancer cells (in vitro) and human glioblastoma tumors (in vivo) [62]. Moreover, Meidanchi et al. [63] reported the possible use of $ZnFe_2O_4$ nanoparticles as radiosensitizers in cancer therapy. Therefore, the obtained nanoparticles in our study can be better explored in biomedical applications including cancer therapy, drug delivery and magnetic resonance imaging in the near future.

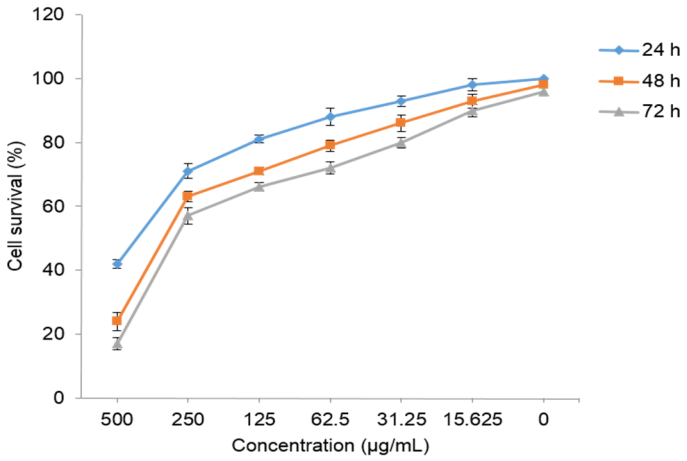

(**a**)

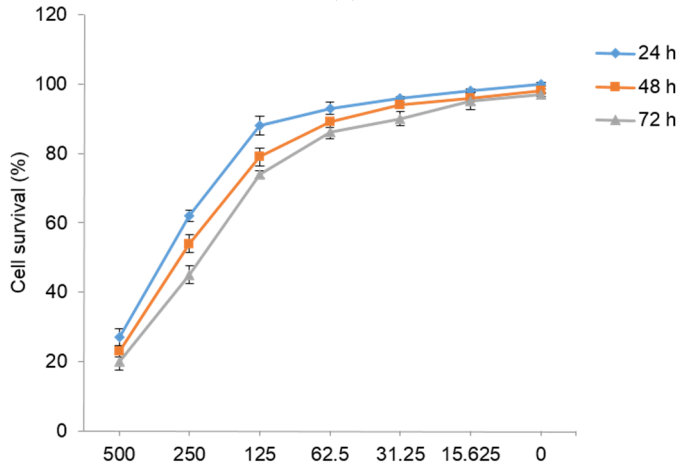

(**b**)

Figure 6. (**a**) The cytotoxic effect of synthesized $CuFe_2O_4$ nanoparticles on MCF-7 cells (human breast cancer cell line). Each value is expressed as a mean of ± S.D (n = 3); (**b**) The cytotoxic effect of synthesized $ZnFe_2O_4$ nanoparticles on MCF-7 cells (human breast cancer cell line).

4. Conclusions

Copper ferrite and zinc ferrite spinel nanoparticles were successfully prepared by the sol-gel self-combustion method. XRD and FTIR results confirm the preparation of nanocrystalline $CuFe_2O_4$ and $ZnFe_2O_4$ nanoparticles. From the TEM results, the synthesized $CuFe_2O_4$ and $ZnFe_2O_4$ nanoparticles are shown to be uniformly distributed and almost spherical in shape. The results of VSM show that the both ferrites exhibit a ferromagnetic nature. Both $ZnFe_2O_4$ and $CuFe_2O_4$ nanoparticles showed appreciable antioxidant activity at lower concentrations. In vitro cytotoxicity study revealed their dose dependent activity against MCF-7 cells with higher toxicity observed at higher concentrations of nanoparticles. Concentrations below 125 μg/mL were found to be less toxic suggesting their biocompatibility at lower concentrations. As these synthesized nanoparticles exhibit biocompatibility associated with superparamagnetism, they can be better explored in the near future for various biomedical applications such as cancer therapy, drug delivery, imaging analysis.

Acknowledgments: We would like to thank Universiti Putra Malaysia for providing the Financial and Center Facilities.

Author Contributions: The experimental work was designed and performed by S.K. under the supervision of S.B.A.A. S.T. and M.K.S. contributed to the biological studies. M.H., N.B.B.M.A., I.I. and S. B.A.A. provided scientific guidance. S.K., B.P.C.R. and M.K.S. drafted the manuscript. All authors read and approved the final manuscript.

Conflicts of Interest: The authors declare no conflict of interest.

References

1. Perez, J.A.L.; Quintela, M.A.L.; Mira, J.; Rivas, J.; Charles, S.W. Advances in the preparation of magnetic nanoparticles by the microemulsion method. *J. Phys. Chem. B* **1997**, *101*, 8045–8047. [CrossRef]
2. Chen, Q.; Zhang, Z.J. Size-dependent superparamagnetic properties of $MgFe_2O_4$ spinel ferrite nanocrystallites. *Appl. Phys. Lett.* **1998**, *73*, 3156–3158. [CrossRef]
3. Tang, Z.X.; Sorensen, C.M.; Klabunde, K.J.; Hadjipanayis, G.C. Preparation of Mn ferrite fine particles from aqueous solution. *J. Colloid Interface Sci.* **1991**, *146*, 38–46. [CrossRef]
4. Seip, C.T.; Carpenter, E.E.; O'Connor, C.J.; John, V.T.; Li, S. Magnetic properties of a series of ferrite nanoparticles synthesized in reverse micelles. *IEEE Trans. Magn.* **1998**, *34*, 1111–1113. [CrossRef]
5. Hochepied, J.F.; Bonville, P.; Pileni, M.P. Nonstoichiometric zinc ferrite nanocrystals: Syntheses and unusual magnetic properties. *J. Phys. Chem. B* **2000**, *104*, 905–912. [CrossRef]
6. Liu, C.; Zou, B.; Rondinone, A.J.; Zhang, Z.J. Reverse micelle synthesis and characterization of superparamagnetic $MnFe_2O_4$ spinel ferrite nanocrystallites. *J. Phys. Chem. B* **2000**, *104*, 1141–1145. [CrossRef]
7. Raghavender, A.T.; Kulkarni, R.G.; Jadhav, K.M. Magnetic properties of mixed cobalt-aluminum ferrite nanoparticles. *Chin. J. Phys.* **2010**, *48*, 512–522.
8. Rajath Varma, P.C.; Manna, R.S.; Banerjee, D.; Varma, M.R.; Suresh, K.G.; Nigam, A.K. Magnetic properties of $CoFe_2O_4$ synthesized by solid state, citrate precursor and polymerized complex methods: A comparative study. *J. Alloys Comp.* **2008**, *453*, 298–303. [CrossRef]
9. Kahn, M.L.; Zhang, Z.J. Synthesis and magnetic properties of $CoFe_2O_4$ spinel ferrite nanoparticles doped with lanthanide ions. *Appl. Phys. Lett.* **2001**, *78*, 3651–3653. [CrossRef]
10. Mohapatra, M.; Anand, S. Synthesis and applications of nano-structured iron oxides/hydroxides—A review. *Int. J. Eng. Sci. Technol.* **2010**, *2*, 127–146. [CrossRef]
11. Zak, T.; Cosovic, V.; Cosovic, A.; David, B.; Talijan, N.; Zivkovic, D. Formation of magnetic microstructure of the nanosized $NiFe_2O_4$ synthesized via solid-state reaction. *Sci. Sinter.* **2012**, *44*, 103–112. [CrossRef]
12. Standley, K.J. *Oxide Magnetic Materials*, 2nd ed.; Oxford University Press: Oxford, UK, 1972.
13. Yattinahalli, S.; Kapatkar, S.B.; Ayachit, N.H.; Mathad, S.N. Synthesis and structural haracterization of nanosized nickel ferrite. *Int. J. Self-Propag. High-Temp. Synth.* **2013**, *22*, 147–150. [CrossRef]
14. Safarik, I.; Horska, K.; Pospiskova, K.; Safarikova, M. Magnetic techniques for the detection and determination of xenobiotics and cells in water. *Anal. Bioanal. Chem.* **2012**, *404*, 1257–1273. [CrossRef] [PubMed]

15. Pospiskova, K.; Safarik, I.; Sebela, M.; Kuncova, G. Magnetic particles-based biosensor for biogenic amines using an optical oxygen sensor as a transducer. *Microchim. Acta* **2013**, *180*, 311–318. [CrossRef]
16. Cui, X.; Belo, S.; Krüger, D.; Yan, Y.; de Rosales, R.T.M.; Jauregui-Osoro, M.; Ye, H.; Su, S.; Mathe, D.; Kovacs, N.; et al. Aluminium hydroxide stabilised $MnFe_2O_4$ and Fe_3O_4 nanoparticles as dual-modality contrasts agent for MRI and PET imaging. *Biomaterials* **2014**, *35*, 5840–5846. [CrossRef] [PubMed]
17. Hou, X.; Feng, J.; Xu, X.; Zhang, M. Synthesis and characterizations of spinel $MnFe_2O_4$ nanorod by seed-hydrothermal route. *J. Alloys Compd.* **2010**, *491*, 258–263. [CrossRef]
18. Shanmugavela, T.; Gokul Rajb, S.; Ramesh Kumarc, G.; Rajarajana, G. Synthesis and structural analysis of nanocrystalline $MnFe_2O_4$. *Phys. Procedia* **2014**, *54*, 159–163. [CrossRef]
19. Zaki, T.; Saed, D.; Aman, D.; Younis, S.A.; Moustafa, Y.M. Synthesis and characterization of MFe_2O_4 sulfur nanoadsorbents. *J. Sol-Gel Sci. Technol.* **2013**, *65*, 269–276. [CrossRef]
20. Kanagesan, S.; Hashim, M.; Tamilselvan, S.; Alitheen, N.B.; Ismail, I.; Syazwan, M.; ZuikimiI, M.M.M. Sol-gel auto-combustion synthesis of cobalt ferrite and it's cytotoxicity properties. *Digest J. Nanomater. Biostruct.* **2013**, *8*, 1601–1610.
21. Qi, X.; Zhou, J.; Yue, Z.; Gui, Z.; Li, L. Permeability and microstructure of manganese modified lithium ferrite prepared by sol-gel auto-combustion method. *Mater. Sci. Eng. B* **2003**, *99*, 278–281. [CrossRef]
22. Yan, S.; Ling, W.; Zhou, E. Rapid synthesis of $Mn_{0.65}Zn_{0.35}Fe_2O_4/SiO_2$ homogeneous nanocomposites by modified sol-gel auto-combustion method. *J. Cryst. Growth.* **2004**, *273*, 226–233. [CrossRef]
23. Mangalaraja, R.V.; Anathakmar, S.; Manohar, P.; Gnanam, F.D.; Awana, M. Characterization of $Mn_{0.8}Zn_{0.2}Fe_2O_4$ synthesized by flash combustion technique. *Mater. Sci. Eng. A* **2004**, *367*, 301–305. [CrossRef]
24. Mangalaraja, R.V.; Anathakmar, S.; Manohar, P.; Gnanam, F.D. Magnetic, electrical and dielectric behaviour of $Ni_{0.8}Zn_{0.2}Fe_2O_4$ prepared through flash combustion technique. *J. Magn. Magn. Mater.* **2002**, *253*, 56–64. [CrossRef]
25. Sileo, E.E.; Jacobo, S.E. Gadolinium-nickel ferrites prepared from metal citrates precursors. *Physica B* **2004**, *354*, 241–245. [CrossRef]
26. Bujoreanu, V.M.; Diamandescu, L.; Brezeanu, M. On the structure of manganese ferrite powder prepared by coprecipitation from MnO_2 and $FeSO_4 \cdot 7H_2O$. *Mater. Lett.* **2000**, *46*, 169–174. [CrossRef]
27. Upadhyay, R.V.; Davies, K.J.; Wells, S.; Charles, S.W. Preparation and characterization of ultra-fine $MnFe_2O_4$ and $Mn_xFe_{1-x}Fe_2O_4$ spinel systems: I. particles. *J. Magn. Magn. Mater.* **1994**, *132*, 249–257. [CrossRef]
28. Shi, Y.; Ding, J.; Liu, X.; Wang, J. $NiFe_2O_4$ ultrafine particles prepared by co-precipitation/mechanical alloying. *J. Magn. Magn. Mater.* **1999**, *205*, 249–254. [CrossRef]
29. Azadmanjiria, J.; Seyyed Ebrahimib, S.A.; Salehania, H.K. Magnetic properties of nanosize $NiFe_2O_4$ particles synthesized by sol-gel auto combustion method. *Ceram. Int.* **2007**, *33*, 1623–1625. [CrossRef]
30. Kanagesan, S.; Hashim, M.; Tamilselvan, S.; Alitheen, N.B.; Ismail, I.; Ismail, M.A.N.; Bahmanrokh, G.; Rahman, M.M. Characteristics and cytotoxicity of magnetic nanoparticles on breast cancer cells. *J. Optoelectron. Adv. Mater.* **2014**, *6*, 41–50.
31. Karimi, Z.; Karimi, L.; Shokrollahi, H. Nano-magnetic particles used in biomedicine: Core and coating materials. *Mater. Sci. Eng. C* **2013**, *33*, 2465–2475. [CrossRef] [PubMed]
32. Akbarzadeh, A.; Samiei, M.; Davaran, S. Magnetic nanoparticles: Preparation, physical properties, and applications in biomedicine. *Nanoscale Res. Lett.* **2012**, *7*. [CrossRef] [PubMed]
33. Sen, S.; Konar, S.; Pathak, A.; Dasgupta, S.; Das Gupta, S. Effect of functionalized magnetic $MnFe_2O_4$ nanoparticles on fibrillation of human serum albumin. *J. Phys. Chem. B* **2014**, *118*, 11667–11676. [CrossRef] [PubMed]
34. Swamy, M.K.; Sinniah, U.R.; Akhtar, M.S. In vitro pharmacological activities and GC-MS analysis of different solvent extracts of *Lantana camara* leaves collected from tropical region of Malaysia. *Evid. Based Complement. Alternat. Med.* **2015**, *2015*. [CrossRef] [PubMed]
35. Swamy, M.K.; Akhtar, M.S.; Mohanty, S.K.; Sinniah, U.R. Synthesis and characterization of silver nanoparticles using fruit extract of *Momordica cymbalaria* and assessment of their in vitro antimicrobial, antioxidant and cytotoxicity activities. *Spectrochim. Acta A Mol. Biomol. Spectrosc.* **2015**, *151*, 939–944. [CrossRef] [PubMed]
36. Das, D.; Nath, B.C.; Phukon, P.; Dolui, S.K. Synthesis and evaluation of antioxidant and antibacterial behavior of CuO nanoparticles. *Colloids Surf. B* **2013**, *101*, 430–433. [CrossRef] [PubMed]

37. Akhtar, M.S.; Swamy, M.K.; Umar, A.; Al Sahli, A.A. Biosynthesis and characterization of silver nanoparticles from methanol leaf extract of *Cassia didymobotyra* and assessment of their antioxidant and antibacterial activities. *J. Nanosci. Nanotechnol.* **2015**, *15*, 9818–9823. [CrossRef] [PubMed]
38. Sahoo, B.; Devi, K.S.P.; Banerjee, R.; Maiti, T.K.; Pramanik, P.; Dhara, D. Thermal and pH responsive polymer-tethered multifunctional magnetic nanoparticles for targeted delivery of anticancer drug. *ACS Appl. Mater. Inter.* **2013**, *5*, 3884–3893. [CrossRef] [PubMed]
39. Sun, J.; Wang, S.; Zhao, D.; Hun, F.H.; Weng, L.; Liu, H. Cytotoxicity, permeability, and inflammation of metal oxide nanoparticles in human cardiac microvascular endothelial cells: Cytotoxicity, permeability, and inflammation of metal oxide nanoparticles. *Cell Biol. Toxicol.* **2011**, *27*, 333–342. [CrossRef] [PubMed]
40. Khanna, L.; Verma, N.K. Synthesis, characterization and in vitro cytotoxicity study of calcium ferrite nanoparticles. *Mater. Sci. Semicond. Process.* **2013**, *16*, 1842–1848. [CrossRef]
41. Kanagesan, S.; Hashim, M.; Tamilselvan, S.; Alitheen, N.B.; Ismail, I.; Bahmanrokh, G. Cytotoxic effect of nanocrystalline $MgFe_2O_4$ particles for cancer cure. *J. Nanomater.* **2013**, *2013*. [CrossRef]
42. Chandradass, J.; Jadhav, A.H.; Kim, K.H.; Kim, H. Influence of processing methodology on the structural and magnetic behavior of $MgFe_2O_4$ nanopowders. *J. Alloys Compd.* **2012**, *517*, 164–169. [CrossRef]
43. Dolci, S.; Domenici, V.; Duce, C.; Tiné, M.R.; Ierardi, V.; Valbusa, U.; Jaglicic, Z.; Boni, A.; Gemmi, M.; Pampaloni, G. Ultrasmall superparamagnetic iron oxide nanoparticles with titanium-*N*,*N*-dialkylcarbamato coating. *Mater. Res. Express* **2014**, *1*. [CrossRef]
44. Krehula, S.; Music, S. Influence of Mn-dopant on the properties of α-FeOOH particles precipitated in highly alkaline media. *J. Alloys Compd.* **2006**, *426*, 327–334. [CrossRef]
45. Iacob, M. Sonochemical synthesis of hematite nanoparticles, chemistry journal of moldova. *Gen. Ind. Ecol. Chem.* **2015**, *10*, 46–51.
46. Tahar, L.B.; Smiri, L.S.; Artus, M.; Joudrier, A.; Herbst, F.; Vaulay, M.J.; Ammar, S.; Fievet, F. Characterization and magnetic properties of Sm- and Gd-substituted $CoFe_2O_4$ nanoparticles prepared by forced hydrolysis in polyol. *Mater. Res. Bull.* **2007**, *42*, 1888–1896. [CrossRef]
47. Deng, H.; Chen, H.; Li, H. Synthesis of crystal MFe_2O_4 (M = Mg, Cu, Ni) microspheres. *Mater. Chem. Phys.* **2007**, *101*, 509–513. [CrossRef]
48. Smit, J.; Wijn, H.P.J. *Ferrites Physical Properties of Ferromagnetic Oxides in Relation to Their Technical Applications*; Wiley: New York, NY, USA, 1959.
49. Kovacic, P.; Somanathan, R. Nanoparticles: Toxicity, radicals, electron transfer, and antioxidants. *Methods Mol. Biol.* **2013**, *1028*, 15–35. [PubMed]
50. Das, D.; Nath, B.C.; Phukon, P.; Dolui, S.K. Synthesis of ZnO nanoparticles and evaluation of antioxidant and cytotoxic activity. *Colloids Surf. B* **2013**, *111*, 556–560. [CrossRef] [PubMed]
51. Paul, S.S.J.P.; Saikia, J.P.; Samdarshi, S.K.; Konwar, B.K. Investigation of antioxidant property of iron oxide particles by 1′-1′ diphenylpicryl-hydrazyle (DPPH) method. *J. Magn. Magn. Mater.* **2009**, *321*, 3621–3623. [CrossRef]
52. Covaliu, C.I.; Matei, C.; Litescu, S.; Eremia, S.A.M.; Stanica, N.; Diamandescu, L.; Ianculescu, A.; Jitaru, I.; Berger, D. Radical scavenger properties of oxide nanoparticles stabilized with biopolymer matrix. *Rev. Mater. Plast.* **2010**, *47*, 5–10.
53. Saikia, J.P.; Paul, S.; Konwar, B.K.; Samdarshi, S.K. Nickel oxide nanoparticles: A novel antioxidant. *Colloids Surf. B* **2010**, *78*, 146–148. [CrossRef] [PubMed]
54. Hussain, S.M.; Javorina, A.K.; Schrand, A.M.; Duhart, H.M.; Ali, S.F.; Schlager, J.J. The interaction of manganese nanoparticles with PC-12 cells induces dopamine depletion. *Toxicol. Sci.* **2006**, *92*, 456–463. [CrossRef] [PubMed]
55. Alhadlaq, H.A.; Akhtar, M.J.; Ahamed, M. Zinc ferrite nanoparticle-induced cytotoxicity and oxidative stress in different human cells. *Cell Biosci.* **2015**, *9*. [CrossRef] [PubMed]
56. Swamy, M.K.; Sudipta, K.M.; Jayanta, K.; Balasubramanya, S. The green synthesis, characterization, and evaluation of the biological activities of silver nanoparticles synthesized from *Leptadenia reticulata* leaf extract. *Appl. Nanosci.* **2015**, *5*, 73–81. [CrossRef]
57. Tomitaka, A.; Hirukawa, A.; Yamada, T.; Morishita, S.; Takemura, Y. Biocompatibility of various ferrite nanoparticles evaluated by in vitro cytotoxicity assays using HeLa cells. *J. Magn. Magn. Mater.* **2009**, *321*, 1482–1484. [CrossRef]

58. Leung, K.C.F.; Wang, Y.X.J. Mn–Fe nanowires towards cell labeling and magnetic resonance imaging. In *Nanowires Science and Technology*; Nicoleta, L., Ed.; In Tech Open Access Publisher: Hong Kong, China, 2010.
59. Gupta, A.K.; Gupta, M. Synthesis and surface engineering of iron oxide nanoparticles for biomedical applications. *Biomaterials* **2005**, *26*, 3995–4021. [CrossRef] [PubMed]
60. Saptarshi, S.R.; Feltis, B.N.; Wright, P.F.; Lopata, A.L. Investigating the immunomodulatory nature of zinc oxide nanoparticles at sub-cytotoxic levels in vitro and after intranasal instillation in vivo. *J. Nanobiotechnol.* **2015**, *13*. [CrossRef] [PubMed]
61. Hajipour, M.J.; Akhavan, O.; Meidanchi, A.; Laurent, S.; Mahmoudi, M. Hyperthermia-induced protein corona improves the therapeutic effects of zinc ferrite spinel-graphene sheets against cancer. *RSC Adv.* **2014**, *4*, 62557–62565. [CrossRef]
62. Akhavan, O.; Meidanchi, A.; Ghaderi, E.; Khoei, S. Zinc ferrite spinel-graphene in magneto-photothermal therapy of cancer. *J. Mater. Chem. B* **2014**, *2*, 3306–3314. [CrossRef]
63. Meidanchi, A.; Akhavan, O.; Khoei, S.; Shokri, A.A.; Hajikarimi, Z.; Khansari, N. $ZnFe_2O_4$ nanoparticles as radiosensitizers in radiotherapy of human prostate cancer cells. *Mater. Sci. Eng. C* **2015**, *46*, 394–399. [CrossRef] [PubMed]